Combining borehole and surface seismic data for velocity field estimation through slope tomography

Adam Gosselet, Soazig Le Bégat

Geophys. J. Int. (2009) **176,** 897–908 doi: 10.1111/j.1365-246X.2008.04022.x

Combining borehole and surface seismic data for velocity field estimation through slope tomography

Adam Gosselet[1,2] and Soazig Le Bégat[1]

[1] *Centre de Géophysique, Mines ParisTech, Fontainebleau, France*
[2] *Institut de Physique du Globe de Paris, Centre de Recherche sur le Stockage Géologique du* CO_2, 4 *place Jussieu, case* 89*, Tour* 14, 2[eme] *étage.,* 75252 *Paris, France. E-mail: soazig.lebegat@orange.fr*

Accepted 2008 October 27. Received 2008 September 8; in original form 2008 February 8

SUMMARY

A joint traveltime and slope (or slowness) tomography method of marine surface reflections and walk-away transmitted arrivals is investigated. Based on our previous developments of 2-D isotropic slope tomography dedicated to reflection data, the transmitted arrivals are added into the inversion scheme. The results of the transmitted arrival tomography are compared to those of the joint (transmitted and reflected arrivals) tomography on synthetic data. Moreover, a quality control (QC) procedure is proposed. Finally, walk-away transmitted arrivals, surface reflected arrivals and joint tomography of both arrivals are applied on real data sets from Oseberg, North Sea. These data include 2-D surface and walk-away lines along the same direction. The resulting velocity fields are used for pre-stack depth migration, allowing us to conclude that joint inversion leads to significantly improved images both in terms of focusing and event location. A key point is that improvements are not restricted in the area covered by transmitted arrivals. As the number of available borehole receivers is small, this case study demonstrates the strong impact direct arrivals that may have on depth imaging.

Key words: Tomography; Body waves; Seismic tomography.

INTRODUCTION

For a decade, seismic data acquisition geometry and procedures have been greatly widened: ocean bottom cable, walk-away and seismic while drilling have become reliable techniques to improve subsurface knowledge. In particular, the combination of data sets allows better subsurface velocity estimation, imaging, and thus interpretation thanks to complementary information brought by each data set. The simultaneous uses of surface and borehole data are more and more showing their worth (Chiu & Stewart 1987; Sexton 1998; Constance *et al.* 1999; Vesnaver *et al.* 1999a; Cao *et al.* 2000; Rossi *et al.* 2001; Chopra *et al.* 2002; Lapin *et al.* 2003; Leaney *et al.* 2003) . In this context, the paper focuses on the joint inversion of *P* waves from walk-away transmitted arrivals and surface reflected arrivals. As they increase spatial and angular coverage of the subsurface, walk-away transmitted arrivals add constraints on the velocity model. The velocity–depth ambiguity is also reduced when using transmitted arrivals: these data provide a direct relationship between average velocity and depth (and thus well tie).

Following our previous works on 2-D isotropic slope tomography (Le Bégat *et al*. 2000; Billette *et al*. 2003; Le Bégat *et al*. 2004), in this paper is included information of borehole transmitted data together with reflection data in a joint optimization process. Compared to traveltime tomography, slope tomography uses the slopes of locally coherent events in addition to traveltime data (Riabinkin 1957; Sword 1986; Billette & Lambaré 1998; Whiting 1998). The use of an event local slope in a gather (common shot or common receiver) provides a direct estimation of a component of the slowness vector. As a local event contains complete information about the reflection geometry, one of the main advantages of slope tomography is to better constrain the velocity model. Moreover, automatic picking of the data is possible in slope tomography: picked events are only required to be locally coherent and there is no need to associate a given event with an interface of the model. Picking may be performed on local slant stack panels and is consequently easier than picking on un-stacked trace gathers. Compared to traveltime tomography where only a few continuous events are usually used, dense picking is feasible in slope tomography. Slope measurements not only make picking automatic but also allow additional data such as reflections from fault planes or diffractions to be used in the inversion process. In traveltime tomography instabilities are associated with singularities or difficulties in ray tracing (multipathing, caustics). Such singularities can be unfolded examining the ray field in the phase space. Ray multipathing can thereby be accounted for since paths are discriminated by their associated slopes. Working on transmitted arrivals, either first or later arrivals (if they can be picked) may be used in the tomography. Estimating the quality of the inverted velocity field is a difficult point in tomography. Based on slopes, we propose to kinematically simulate the migration of borehole transmitted arrivals generating depth 'focusing diagrams'.

These diagrams provide an estimation of focusing and well tie for a given velocity model. As only a few rays need to be traced, this quality control (QC) is very fast. Finally, since the picking is based on the hypothesis of primary events, it does not solve problems linked to other arrivals (refracted, multiples, low-amplitude. . .) but the slope could be used as a sort-out criterion.

The first part of the paper presents the slope tomography method and its extension to the joint inversion of reflected and transmitted data. Validation tests are then provided. Finally, the joint tomography is applied to a real data set from the Oseberg field, North Sea, in comparison with separated walk-away data and surface data tomographies.

SURFACE DATA SLOPE TOMOGRAPHY

In standard reflection traveltime tomography, a layer cake model made of interfaces and velocity fields in between is ordinarily used. As interfaces are defined through the whole model, reflected events have to be picked continuously through the whole seismic section. Such a manual and interpretative approach may be very difficult and time consuming in complex areas. Picking locally coherent events (coherent signals over a few traces) is thus a way to overcome this difficulty: only available information is picked, no interpretation is required, and local events can be automatically picked (Sword 1986; Whiting 1998). Diffractions can also be picked and used in the tomography. As with other tomographic methods, slope tomography uses primary events and assumes that multiples were successfully removed from the data set.

A locally coherent event is entirely defined by its source and receiver locations, traveltimes and slopes. In the example of source–receiver pairs (Fig. 1), if the receivers are close enough, wave fronts can be considered as locally plane and rays are parallel. The horizontal component of the slowness vector at the receiver location is

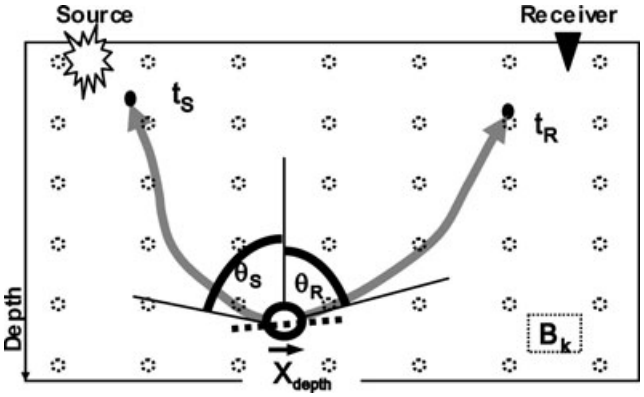

Figure 2. In slope tomography, each locally coherent event picked in the data set is associated to a reflecting/diffracting point $\mathbf{X}_{\text{depth}}$ in depth. The modelling then consists in tracing rays from the depth point towards source and receiver, according to initial angles θ_S and θ_R, in the current velocity field defined by B-splines knots B_k (circles on the figure). The dip bar (dashed line) indicates the local geological dip.

then:

$$p_x = \|\mathbf{p}\| \cdot \cos(\theta) = \frac{\cos(\theta)}{V} = \frac{\mathrm{d}t}{\mathrm{d}x} \tag{1}$$

which is equal to the apparent slope of the corresponding locally coherent event measured in the common source gather (Fig. 1). Similarly, the slope at source can be measured in the common receiver gather. Therefore, measuring the apparent slope in the time domain provides one component of the slowness vector. Because of such a direct link, the slowness vector will be called slope as well. Traveltimes and slopes are measured using an automatic picking tool based on local slant stacks (Billette *et al.* 2003). The slope tomography data set consists in N picked locally coherent events:

$$D^{\text{pick}}_{\text{surface}} = \left\{ \left(\mathbf{X}^i_{\text{S}}, \mathbf{X}^i_{\text{R}}, P^i_{\text{S}}, P^i_{\text{R}}, T^i_{\text{SR}} \right)_{i=1,N} \right\} \tag{2}$$

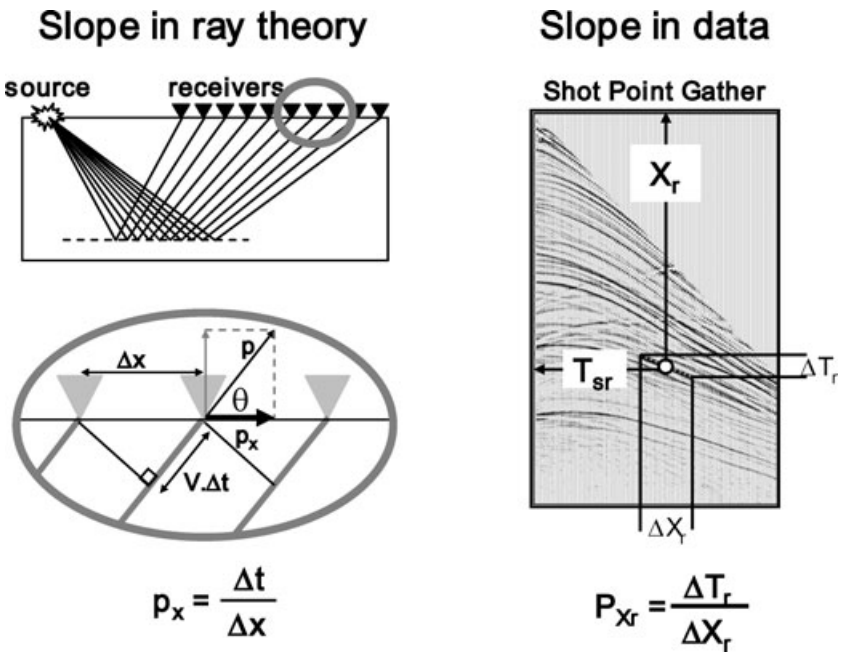

Figure 1. The horizontal component of the ray parameter p_x (left-hand side) can be related to the apparent slope P_{X_r} measured in a common shot (or common receiver) gather. A locally coherent event is defined by the receiver (and source) coordinate X_r, the two-way traveltime T_{SR}, and the slopes picked in common shot and common receiver gathers.

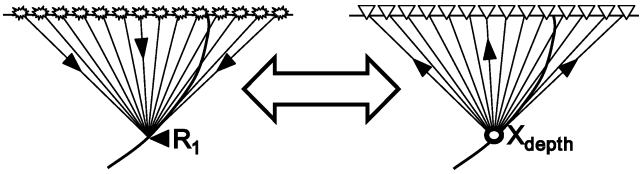

Figure 3. Based on the reciprocity principle, walk away data transmitted from the surface and recorded at a given receiver R_1 are equivalent to data recorded at the surface and coming from a diffracting point $\mathbf{X}_{\text{depth}}$.

with $\mathbf{X}_{\text{S}}^{i}$ the source locations, $\mathbf{X}_{\text{R}}^{i}$ the receiver locations, P_{S}^{i} the slopes at sources, P_{R}^{i} the slopes at receivers and T_{SR}^{i} the two-way traveltimes.

Modelling in slope tomography consists in shooting rays in a smooth velocity field from a common depth point $\mathbf{X}_{\text{depth}}$ towards the source and the receiver, according to given take-off angles θ_{S} and θ_{R} (Fig. 2). The upward propagation is over when one-way traveltimes t_{S} and t_{R} are reached. The tomographic model parameters are then:

$$M_{\text{surface}} = \left\{ \left(\mathbf{X}_{\text{depth}}^{i}, t_{\text{S}}^{i}, \theta_{\text{S}}^{i}, t_{\text{R}}^{i}, \theta_{\text{R}}^{i} \right)_{i=1,N}, \quad (B_k)_{k=1,N_{\text{V}}} \right\} \tag{3}$$

with B_k for the N_{V} B-Splines knots describing the velocity field. As more picks are added more parameters must be taken into account. This leads to a larger (but still sparse) tomographic matrix.

Following the inverse problem formulation proposed by Tarantola (1987), the inverse problem is thus solved including uncertainties and regularization. Regularization is critical in tomography as it must ensure inversion convergence. But due to restricted illumination of the target, seismic tomographic systems are generally ill-conditioned, even if overdetermined. Following Ory & Pratt (1995), finite difference operators are used here to define velocity smoothing. The tomographic matrix is inverted by LSQR iterative conjugate gradient algorithm of Paige & Saunders (1982), updating simultaneously ray segment parameters and velocity parameters. The final slope tomographic outputs are a smooth velocity field plus a depth migrated skeleton (described by local dip of reflected events).

JOINT REFLECTION AND TRANSMISSION TOMOGRAPHY

In opposition to reflections, transmissions do not require any reflection/diffraction depth point parameter since only continuous paths from source to receiver are involved. To keep the same formalism as for reflected data, transmitted arrivals could be described with a virtual depth point $\mathbf{X}_{\text{depth}}$ located somewhere along the ray. Nevertheless, we propose to analyse the transmitted arrivals in common receiver gathers (Fig. 3). Kinematically, these gathers are

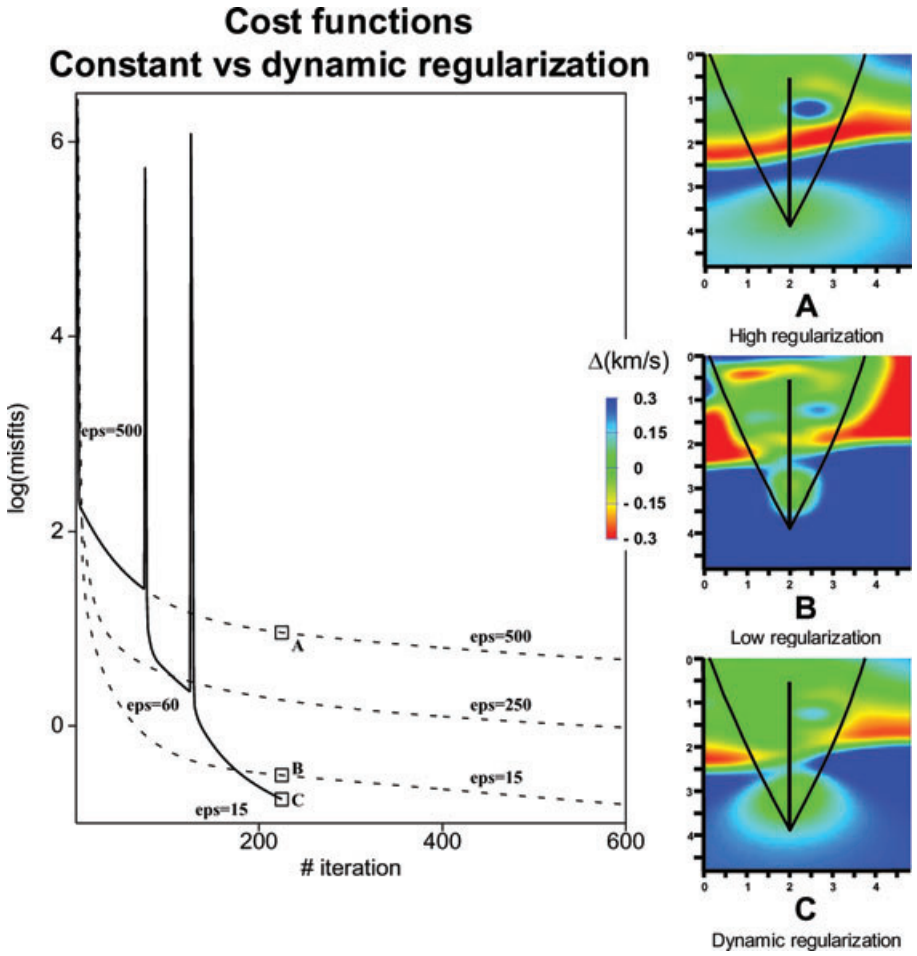

Figure 4. Constant versus dynamic regularization in the case of noise-free inversion of synthetic picks. The dashed lines display misfit functions corresponding to inversions using constant smoothing factors (eps). The solid line displays a dynamic series of decreasing smoothing factors providing faster convergence. The differences between exact and inverted velocity models at points A, B and C are shown on the right-hand side. Cones indicate the area covered by transmitted rays.

equivalent to a diffraction occurring at the borehole receiver location and recorded at the surface (Fig. 3). The receiver location can thus be considered a common depth point parameter shared by a set of rays, instead of two rays for reflections.

In the case of an acquisition involving N_r receivers in the borehole, the data set is then the following:

$$D^{\text{pick}}_{\text{transm}} = \left\{ \left(\left(\mathbf{X}_S^{gj}, P_S^{gj}, T_S^{gj} \right)_{j=1,N_d(g)} \right)_{g=1,N_r} \right\} \quad (4)$$

with

(1) $\mathbf{X}_S^{gj}$ the source location of the jth transmitted arrival reaching the gth borehole receiver;
(2) P_S^{gj} the slopes picked at sources;
(3) T_S^{gj} the one-way traveltimes;
(4) $N_d(g)$ is the number of transmitted arrivals picked in the gth receiver gather.

A strong advantage of the 'gathering approach' is its full consistency with the surface data tomography. First, the same modelling can be used (upward ray tracing from depth). Second, all the arrivals transmitted to the same receiver reach exactly the same point in depth. This information is always true even if the borehole location is doubtful. The chosen parametrization makes implementation of constraints on receiver locations very easy. For instance, the measurement uncertainties on borehole receiver locations can be taken into account. The receiver position may also be fixed (absolutely known) or totally free depending on the deviation survey reliability. The tomographic method is then able to invert the borehole trajectory (Gosselet *et al.* 2004). This last point may be of importance in the case of long distance deviated drilling and borehole positioning. Third, the slope measurement of transmitted data at receiver location is not needed to constrain the ray geometry. However, it can be included as additional or *a priori* information when measurement is feasible. In this case, precise information on the local velocity in the close vicinity of the borehole is available.

Data picking is based on the same local slant stack approach as for surface data. Picking is performed on common receiver gathers to measure traveltimes and local slopes. The corresponding set of parameters can be written as

$$M_{\text{transm}} = \left\{ \left(\mathbf{X}^g_{\substack{\text{depth}\\\text{borehole}}}, \left(t_S^{gj}, \theta_S^{gj}, \right)_{j=1,N_d(g)} \right)_{g=1,N_r}, \quad (B_k)_{k=1,N_V} \right\} \quad (5)$$

with

(1) $\mathbf{X}^g_{\substack{\text{depth}\\\text{borehole}}}$ the depth point parameters, corresponding to the gth receiver location in the borehole;
(2) t_S^{gj} the one-way traveltimes towards sources;
(3) θ_S^{gj} the take-off angles towards sources;
(4) B_k the N_V B-Splines knots describing the velocity field.

The traveltime is specific since it appears both in data and model spaces, with T_S^{gj} and t_S^{gj} not being equal due to measurement uncertainties. When the joint tomography (transmissions and reflections) is performed, the B_k velocity parameters are shared and both data sets contribute to the same velocity field optimization:

$$M_{\text{surface+direct}} = \left\{ \left(\mathbf{X}^i_{\text{depth}}, t_S^i, \theta_S^i, t_R^i, \theta_R^i \right)_{i=1,N}, \right.$$
$$\left. \left(\mathbf{X}^g_{\substack{\text{depth}\\\text{borehole}}}, \left(t_S^{gj}, \theta_S^{gj} \right)_{j=1,N_d(g)} \right)_{g=1,N_r}, (B_k)_{k=1,N_V} \right\}. \quad (6)$$

Without any specific weighting being applied, the joint optimization of the whole data is then performed. Thus, the tomography is data-driven. The final outputs are a unique smooth velocity field plus a depth migrated skeleton. They are now intrinsically consistent with borehole location.

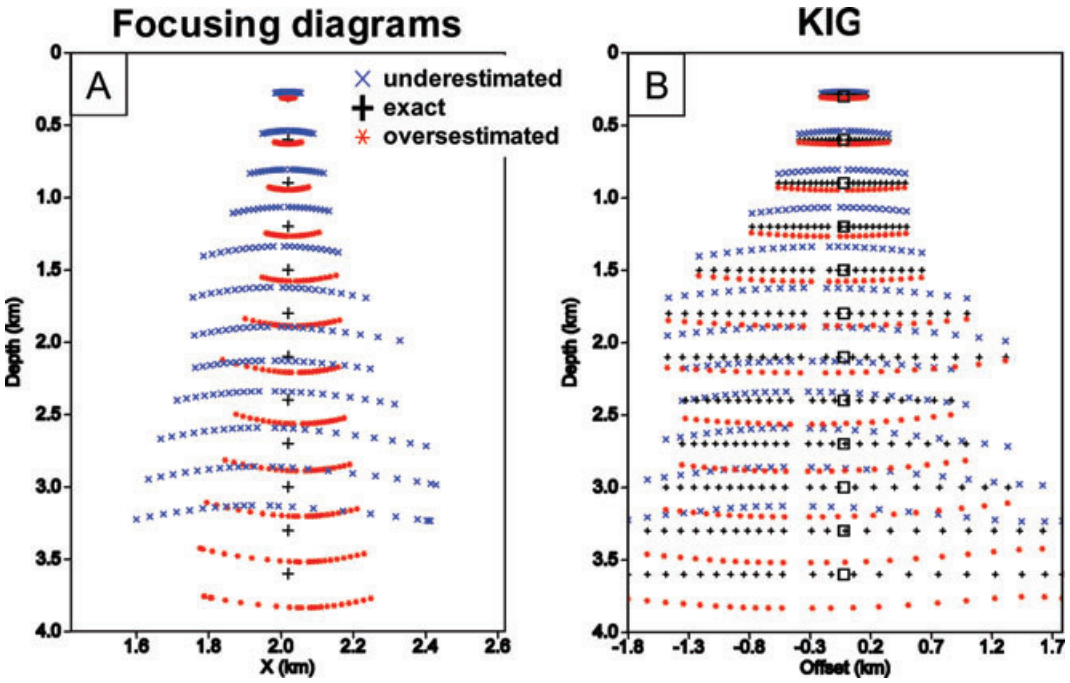

Figure 5. Example of focusing diagrams obtained in underestimated (−10 per cent, blue) and overestimated (+5 per cent, red) models (left-hand side), and associated representation in the offset domain, KIG (right-hand side).

TOMOGRAPHY VALIDATION ON SYNTHETIC PICKS

Model and picks

The 'gathering approach' is first validated on synthetic picks. Transmitted rays are modelled from a vertical borehole into a smooth velocity field considered as the true velocity model. The computed locations, times and slopes make up the input data set for tomography. For consistency, picks computation and forward modelling of the tomography are based on the same ray tracing algorithm. Moreover, the true synthetic and the inverted models have the same parametrization to eliminate numerical discrepancies. The test involves a 5 km × 5 km model containing two layers separated by a sharp velocity gradient and including a local perturbation. The distance between two velocity knots is 200 m vertically and 400 m laterally.

Twelve receivers are located in a borehole, from 0.3 to 3.6 km depth every 300 m, from where 264 rays are computed (leading to 1080 transmitted data). The total number of model parameters is 957 (405 B-Splines knots and 552 ray parameters). The surface reflection picks are generated from a regular grid of depth points (200 m laterally by 400 m vertically). Inversions start from a constant 2.5 km s^{-1} velocity corresponding to average exact velocities.

Regularization

It is well known that seismic tomography is an ill-conditioned inverse problem due to limited illumination of the medium. Therefore, regularization is required to avoid numerical instabilities and velocity artefacts. On the other hand, regularization should be as small as possible to let the data drive the inversion as much as possible. As the choice of relevant regularization remains debatable, many different approaches have been proposed (Sen & Roy 2003). Here,

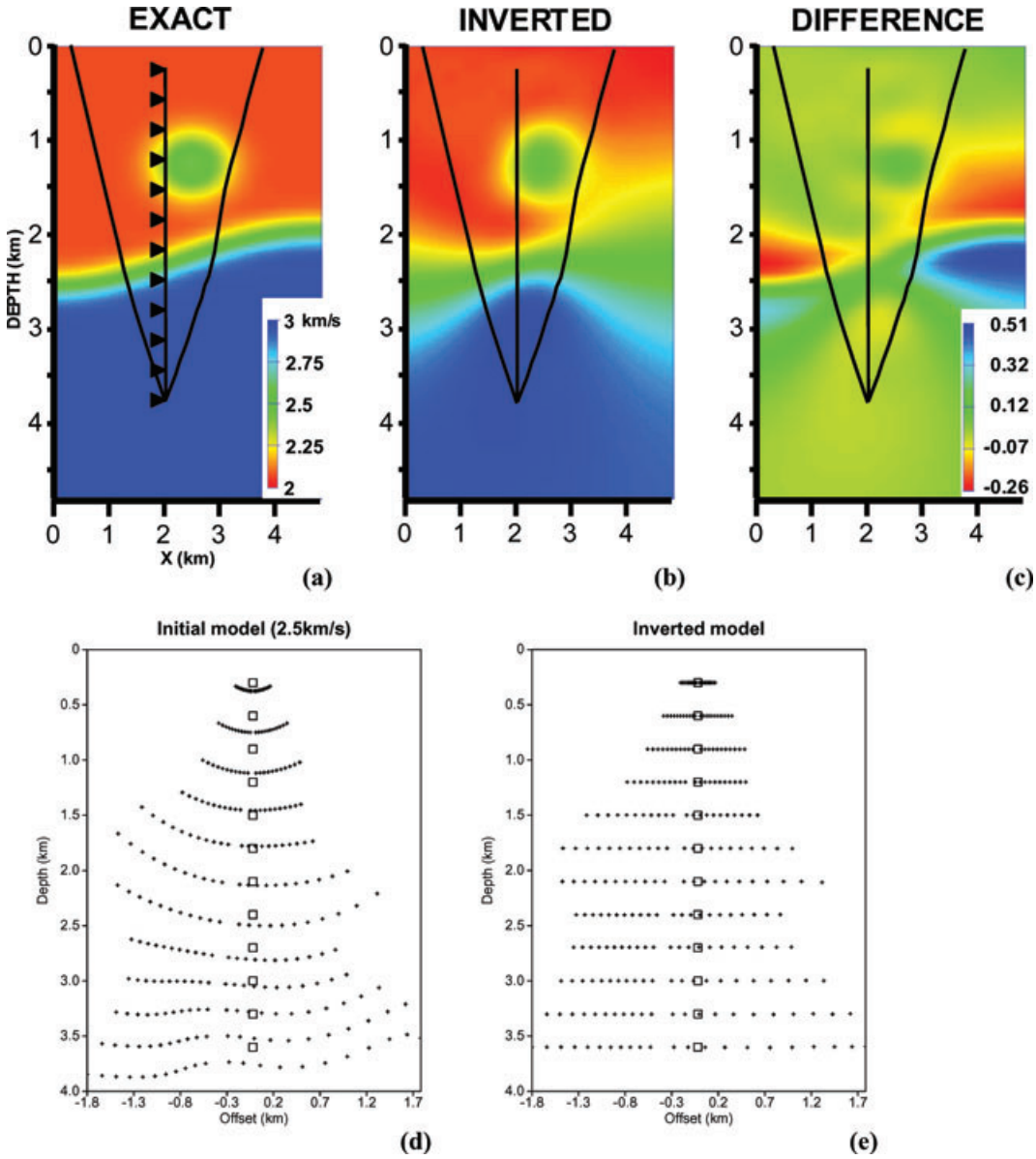

Figure 6. Walk-away synthetic transmitted arrival tomography. (a) Exact model; triangles locate receivers in the vertical borehole; black lines define the ray coverage. (b) Inverted model. (c) Difference between exact and inverted velocity models. KIGs obtained (d) in the initial and (e) inverted velocity fields.

the dynamic continuation approach described by Bube & Langan (1994) is used: the regularization factor is progressively reduced until a low regularization level that does not compromise inversion stability is reached. As a key point is how to decrease the regularization factor, various configurations are tested. Fig. 4 shows misfits versus iterations in the case of transmitted arrival inversion using different regularization factors (dashed lines) and dynamic regularization (solid line). In this noise-free context, the continuation approach provides faster convergence. Differences between exact and inverted models (Fig. 4) show that (1) high regularization ensures inversion stability but poor convergence (strong exact model footprint), (2) low regularization provides lower misfits but leads to unrealistic roughness of the velocity field and (3) dynamic regularization allows simultaneously a small footprint and satisfying convergence.

Quality control

As tomography provides velocity models for seismic data migration, the model quality is essential. The focusing of pre-stack migrated

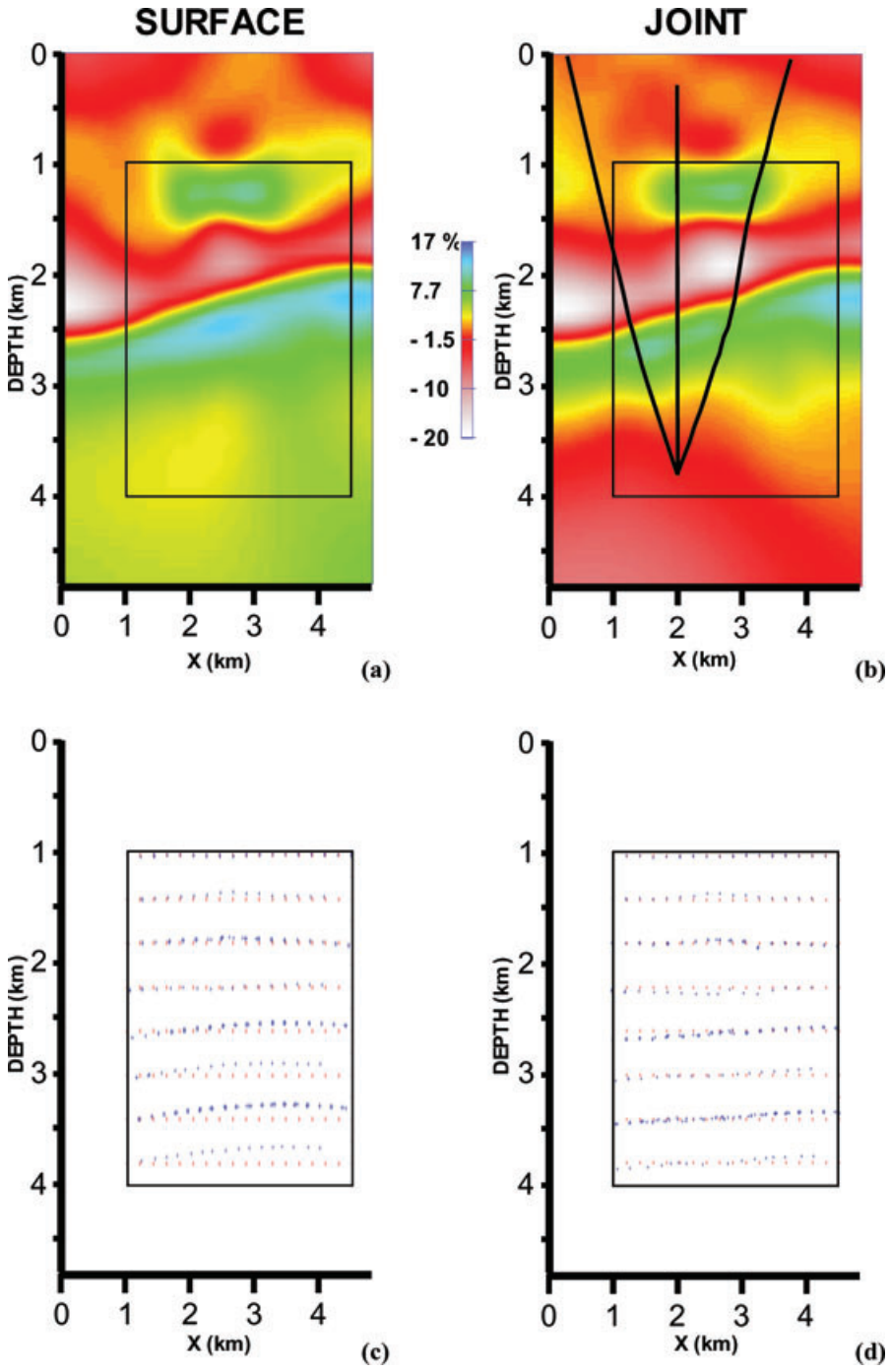

Figure 7. Difference obtained between exact and inverted velocity models through (a) surface tomography and (b) joint tomography. The black line cone describes the transmitted data illumination. The exact reflecting/diffracting depth point locations associated to surface picks are represented by red dots when inverted ones are blue dots for (c) surface tomography and (d) joint tomography.

Table 1. Dynamic regularization applied to synthetic picks joint inversion.

Number of iterations	Smoothing factor
40	500
30	250
20	125
10	60
5	30
5	15
5	10

images is commonly used to control the quality of the velocity model. This is the basic concept used in residual curvature analysis or migration velocity analysis (Al-Yahya 1989; Xu *et al.* 2001; Robein 2004). Such as it has been already described, the reciprocity principle allows to parallel seismic signals recorded in the borehole with signals generated in depth by a diffracting point. While migrating, such signals should exactly reach the borehole receiver location. This location can then be considered a common image point. Measuring the slopes from transmitted arrivals allows to simulate kinematically such a migration. Thus, the focusing capability of the velocity field along the borehole may be estimated.

For each transmission are measured a source location, a one-way traveltime and a slope at source. Using these measurements, rays can be backpropagated downwards from the surface in a given velocity field and stopped when the picked one-way traveltimes are reached. In the case the velocity field is accurate the rays corresponding to the same receiver should reach the same location in depth. If not, spreading will occur corresponding to misfocusing due to erroneous velocities. In the case of imperfect picks, relating blur to either velocity or picking errors will be impossible. Fig. 5 illustrates this purpose in under- and overestimated models: misfocusing, scattered points and well-tie errors are then observed. Hereafter, such figures will be called depth 'focusing diagrams'. In the offset domain, downward patterns can be seen in case of overestimated velocities while upward trends can be seen in case of underestimated velocities (Fig. 5). The exact velocities provide flatness. These curves will be called 'Kinematic Image Gathers' (KIGs).

Transmission tomography

Fig. 6 displays the exact model (Fig. 6a) versus the model recovered from transmitted data (Fig. 6b). In the illuminated area, the perturbation is correctly located but its velocity is overestimated (Fig. 6c). Outside the illuminated area, the velocities change according to smoothing (regularization). Initial KIGs (Fig. 6d) are not flat, indicating that the initial constant velocity field is not correct. Smooth oscillations related to velocity structure can be observed at the three last locations. In comparison, model optimization (even if not perfect) can provide flatness, focusing and well tie (Fig. 6e). From this example, we may conclude that the method allows to recover the velocity field when using noise-free data and appropriate regularization.

Joint tomography

The inversion of reflected data is initiated with a 2.5 km s^{-1} velocity model and a perturbed depth point grid (lateral and vertical 200 m shifts added by 0–50 m random shift per gridpoint). Thanks to the limited size of the inverse problem, a trial-error procedure allows to determine a dynamic regularization sequence (Table 1). Finally, no specific weighting was applied to the two data sets to perform a data-driven joint optimization.

Fig. 7 shows differences between exact and inverted models, these based on surface data inversion (Fig. 7a) and joint inversion (Fig. 7b). Roughly, the red, orange and yellow colours relate to good results while white and blue show poor results. Figs 7c and d compare depth point parameter locations associated to surface picks (blue dots) after surface and joint inversions have taken place. Red dots correspond to the exact depth parameter grid. As the velocity field is not perfectly recovered, blue and red dots do not coincide (Fig. 7c). Adding transmitted arrivals in the inversion provides improvement (Fig. 7d) particularly in the vicinity of the borehole.

REAL DATA FROM NORTH SEA

In this section, the influence and the contribution of walk-away transmitted arrivals in the tomography is investigated on real data. The results of borehole transmitted, surface reflected/diffracted and joint tomographies will be compared and analysed in terms of well ties, velocity models and migrated images.

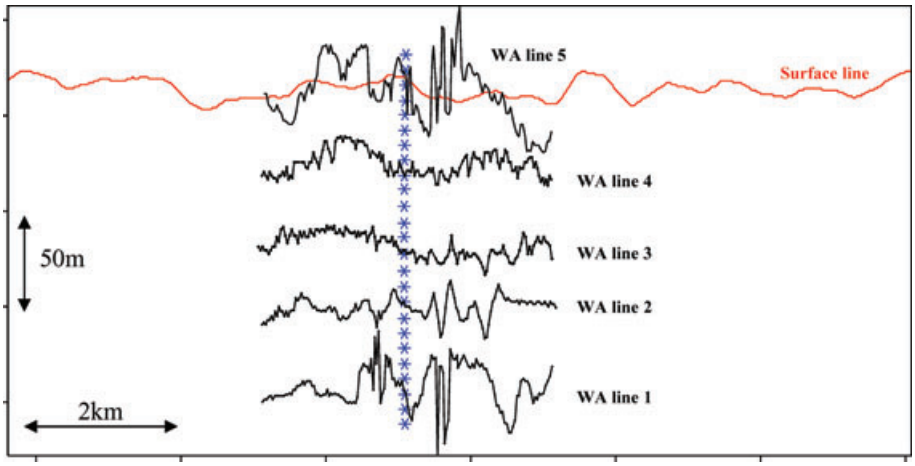

Figure 8. Real data acquisition geometry. Map view of the surface seismic line (red), the walk-away lines (black) and receiver locations in the deviated borehole (blue stars).

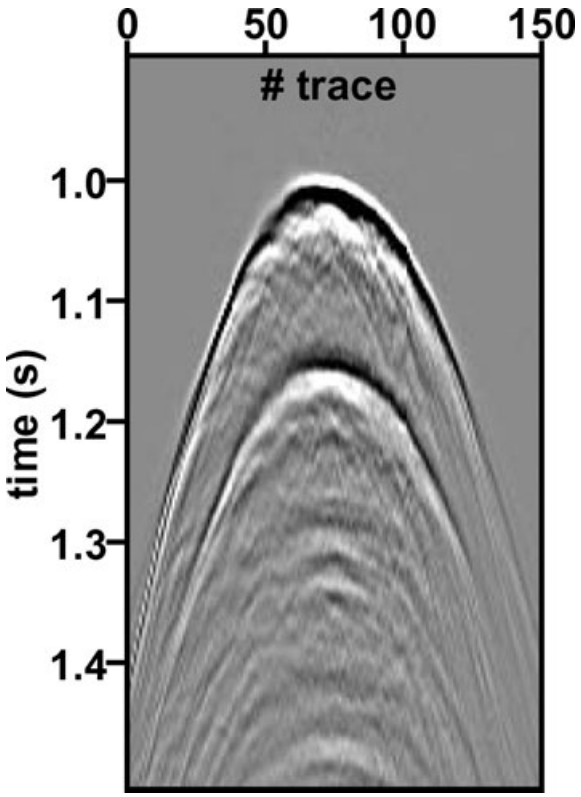

Figure 9. Real walk-away common receiver gather from line 5. Continuous transmitted arrivals, triplications and diffractions may be observed.

Data set description and picking

The two data sets come from the Oseberg field in the North Sea. They have both been pre-processed by Norsk-Hydro for joint imaging of the area. The surface data are made of five adjacent EW 2-D lines with about 40 m spacing. One of the five lines, reaching 12 km long is used in this study (Fig. 8). The 500 shotpoints and the 120 receivers are spaced 25 and 20 m, respectively. The offsets range from 120 to 3.1 km. The walk-away borehole acquisition shows smaller lines centred on the well, following closely the surface reflection seismic navigation (Fig. 8): the five lines are about 4 km long with 151 shotpoints and 25 m spacing. Each sailed source line is associated to one location of the receiver tool (five levels, 15 m spacing) in the borehole, and from 2 to 2.5 km depth. Therefore, the borehole data set is reduced to 25 receiver locations. Moreover, even if the surface and borehole data sets have parallel source lines, they do not lie in the same plane as the borehole. Consequently, for a 2-D demonstration of the method, only one receiver position is theoretically available for each source line reducing much more the walk-away data set.

Traveltimes and slopes of 2500 reflected/diffracted locally coherent events have been automatically picked in the surface seismic data. Transmitted arrivals recorded in the borehole (Fig. 9) have been picked using an interactive tool similarly based on local slant stacks. All events exhibiting signal with enough amplitude and coherence are taken into account. Thus, in case of multipathing the first arrival and/or later arrivals may be picked. As all of them are transmissions (with different slopes), they can be accounted for in the slope tomography. The picked traveltimes and slopes at source are shown on Fig. 10 exhibiting continuous hyperbola shape for traveltimes when slopes present undulations. As slope oscillations are very similar on lines 4 and 5, while shot positions are not, they can be related to velocity heterogeneities.

Tomographic inversions

Inversions are carried out with first borehole transmitted arrivals only, second surface data only and third both data sets jointly. Each tomography starts from a homogeneous (2 km s^{-1}) velocity field. The initial ray parameters are estimated from equivalent media (Billette et *al.* 2003). As transmitted arrivals mainly propagate vertically, the velocity grid knots are 187 m laterally spaced and 500 m

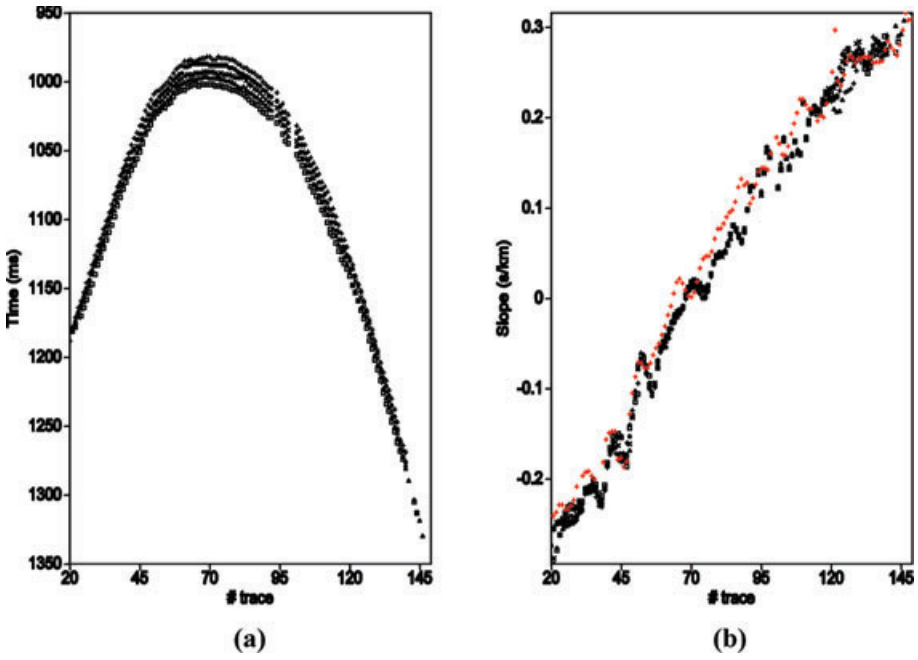

Figure 10. Real data (a) traveltimes picked from walk-away line 5 and (b) slopes picked from line 5 (black) and line 4 (red).

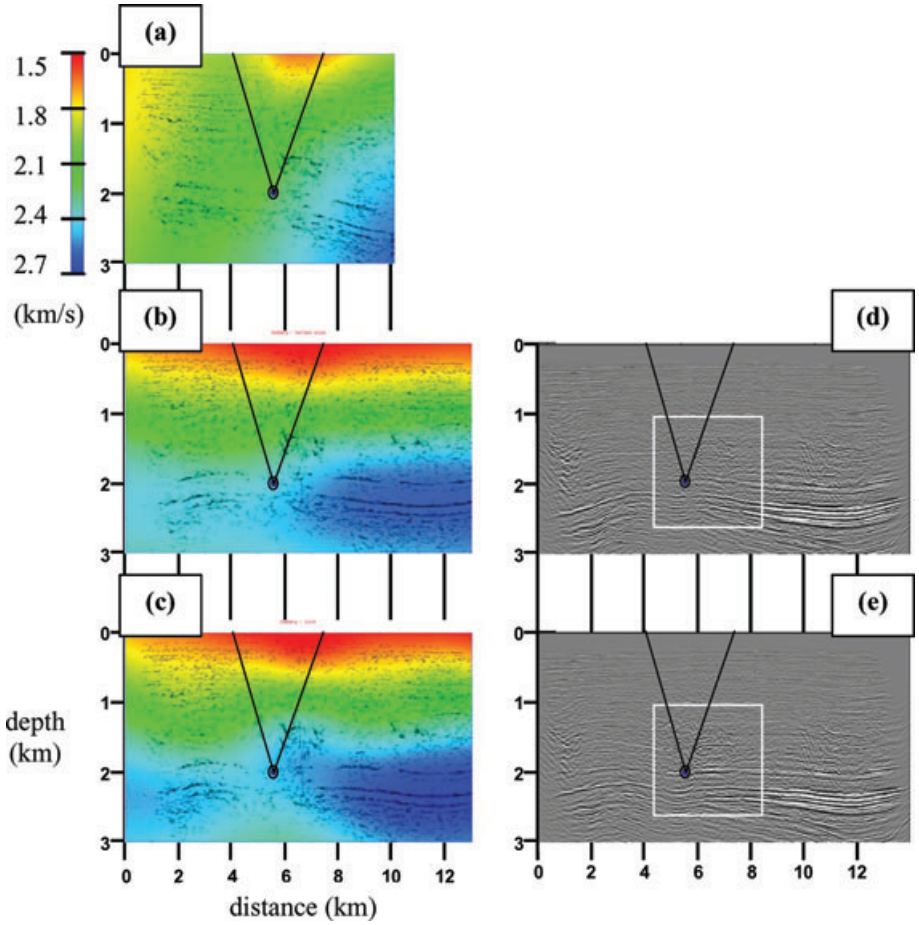

Figure 11. Real data tomography. Models obtained through (a) walk-away transmission tomography, (b) surface reflection tomography and (c) joint tomography. Depth migrated images computed with (d) the surface tomography model and (e) the joint tomography model. The black line cone corresponds to illumination of borehole transmissions.

vertically spaced. When inverting surface data, the vertical sampling is improved and a larger area is covered. Thus, a grid of 750 m laterally and 250 m vertically is used for surface and joint tomographies.

When working with real data, the regularization method used previously for synthetic data is not easily applicable. The dynamic smoothing sequence is thus determined using (1) Wang's (1993) criteria to roughly estimate the smoothing factor, (2) the L-curve (Pratt & Chapman 1992) to determine the smoothing value and (3) depth focusing diagrams.

In this data application, the borehole trajectory is assumed to be known.

Borehole transmitted tomography

The velocity model obtained in the well vicinity through transmitted tomography (Fig. 11a) exhibits distortions due to limited and non-uniform coverage. The information on velocity is not surprisingly centred close to the borehole. However, when positioning the local dips of reflected data in this model, it can be observed that most of the reflections are aligned providing a skeleton of the subsurface structure. Shallower than receiver locations (up to 1.5 km depth) the local dips appear scattered. On the other hand, the proposed model provides satisfying focusing panels (Fig. 12). When points focus in the vicinity of the receiver locations an acceptable convergence is obtained. This application clearly demonstrates once more (1) that transmission tomography can generate an equivalent model insuring well tie but (2) that walk-away acquisition geometry (involving few deep receivers) is unable to provide realistic velocity fields (Rossi *et al.* 2001).

Surface reflected tomography

The velocity model obtained by reflected/diffracted tomography does not exhibit distortions thanks to a wider and more homogeneous coverage of the medium (Fig. 11b). The structural skeleton shows strong interfaces (local dips alignment) from 2 to 2.5 km depth. Discontinuities in the central part of the model are probably due to an overlying complex zone revealed by diffractions (star-like local dips). A focusing panel can be obtained by tracing transmitted rays in the reflection velocity model. As the velocity model is derived from surface data, no information is intrinsically obtained about the borehole location. Thus focusing is not obtained close to the receivers and shallower velocities appear underestimated (Fig. 12). Neither focusing nor well tie can be seen.

Joint tomography

From the previous sections, we came to the conclusion that walk-away transmission tomography converges towards a non-realistic velocity model but ensures a well tie. On the other hand, reflection

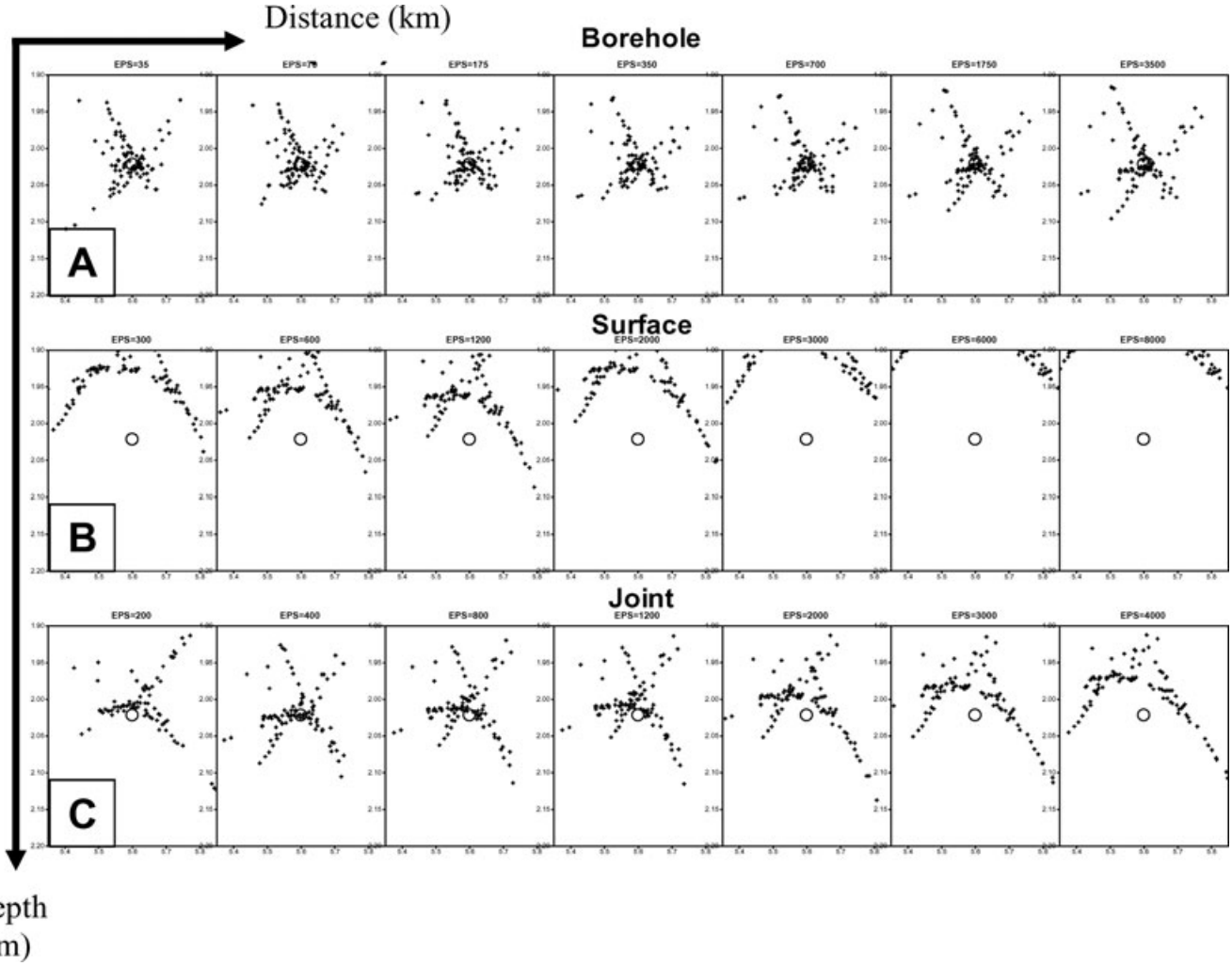

Figure 12. Focusing diagrams obtained in the walk-away tomography model (top), in the surface tomography model (middle) and in the joint tomography model (bottom). Series of smoothing factors are adapted to each inversion.

tomography allows to recover the subsurface structures but does not tie the well. To reach both objectives, borehole transmitted events and surface reflected/diffracted events are jointly inverted. Even if many more surface data than borehole data are usually available, no weighting has been introduced to balance the two data types to avoid reinforcing their contributions artificially. The tomography is then data-driven.

The velocity model obtained from joint inversion (Fig. 11c) shows structures comparable to previous models but they are shifted downwards. At the same time, the use of surface data avoids strong distortions. A slight improvement of local dip focusing in the complex central area is observed. The focusing panel of Fig. 12 confirms that influence of borehole arrivals leads to an acceptable well tie when using adapted regularization. Compared to previous panels, neither focusing nor well tie is as good as those obtained with transmitted arrivals, probably due to model parametrization differences. On the other hand, compared to surface tomography smoothing does ensure acceptable focusing and well tie.

So, the joint inversion accounts for both direct and reflected data contributions. Consequently, improvements on the reflector depth location are observed when suitable regularization is applied. A significant contribution from borehole transmissions is obtained with only a few closely spaced receivers, which is very far from ideal acquisition geometry in tomography. Finally, the impact of borehole seismic data can be observed without applying any weight.

Pre-stack depth migration

To estimate the impact of transmitted arrivals on imaging, pre-stack depth migrations (Nguyen *et al.* 2002) of the surface seismic data were performed with both the velocity models obtained through reflection data (Fig. 11b) and through joint inversion (Fig. 11c). The final migrated sections show flatter reflectors when using the joint tomography model (Fig. 11d) than the image obtained with the surface tomography model (Fig. 11e). This is consistent with geology indicating a mainly tabular structure (Vesnaver *et al.* 1999b). A comparative zoom of the migrated sections centred on the borehole vicinity is shown (Fig. 13). Reflector continuity and location are improved between 2 and 2.5 km depth with joint inversion (Fig. 13b) compared to the image obtained with the reflection velocity model (Fig. 13a). Strong shifts greater than 100 m in depth may be observed. As the borehole receivers are only located from 2 to 2.5 km in depth, the transmitted arrivals do not contribute to improve the migrated section in the shallow area where multiples and anisotropy are suspected. However, the influence of the transmitted arrivals spread far away from the borehole.

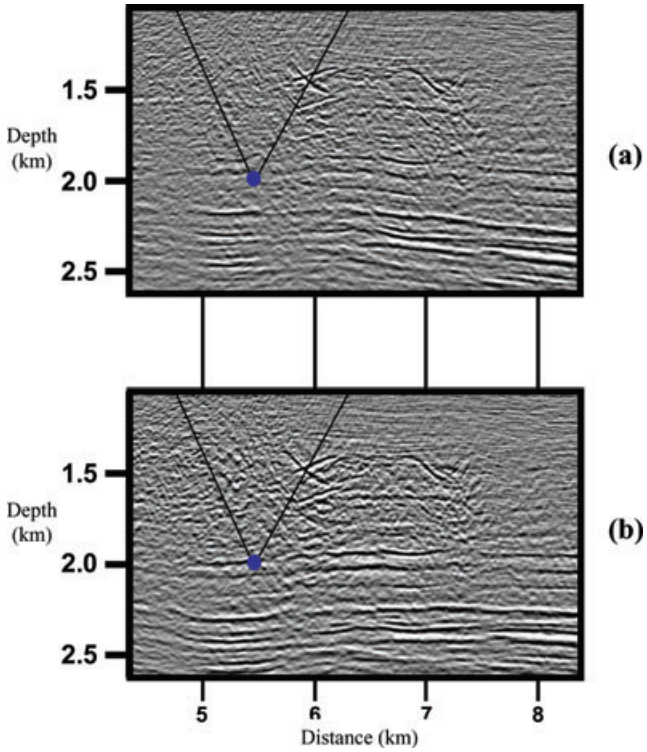

Figure 13. Zoom of depth migrated images computed with (a) the surface tomography model and (b) the joint tomography model. The black line cone corresponds to illumination of borehole transmissions.

CONCLUSION

Surface seismic tomography suffers from the well-known velocity–depth ambiguity problem. So, including borehole data as constraints is essential for the important task of producing seismic images that tie the well. Combining borehole transmissions and reflections in isotropic slope tomography, to obtain a single velocity model, is exemplified. Based on the reciprocity principle, direct arrivals recorded at a given borehole receiver are considered as kinematically equivalent to a diffracting point. Such a gathering allows keeping the same formalism as for reflection tomography. To perform a data-driven joint optimization, no weighting is applied to balance transmitted and reflected data. Finally, thanks to direct arrival slope measurements, a fast QC of tomographic results is feasible: kinematic simulations of depth migration, called focusing diagrams, reveal the focusing capability of the velocity model.

The joint tomography applications to synthetic picks have demonstrated that borehole direct arrivals add value in constraining velocity models: the joint inversion does improve well tie and reduces velocity–depth ambiguity. On real data sets from Oseberg, North Sea, the transmission tomography was able to provide both well tie and focusing in the borehole vicinity. However, the velocity model is not satisfying due to a lack of receivers (and thus coverage) in the shallowest part. On the other hand, compared to reflection tomography, the joint inversion leads to better pre-stack depth migrated images thanks to the borehole data contribution. Both focusing and reflector depth are clearly improved. A key point is that improvements are not restricted to the close vicinity of the well but spread away, particularly below the borehole. This demonstrates the value of borehole seismic data even when very few closely spaced receivers are added to the standard reflection seismic.

ACKNOWLEDGMENTS

The authors thank an anonymous reviewer and Ivan Psencik for their very constructive comments. We are grateful to Hydro for providing and pre-processing the data, and permission to publish the results. We warmly thank Steen A. Petersen (Hydro) for his permanent support and constructive discussions. The work presented in this paper was partly funded by the DIG Consortium sponsors (Bp, Hydro, SGI, Total).

REFERENCES

Al-Yahya, K., 1989. Velocity analysis by iterative profile migration, *Geophysics,* **54,** 718–729.

Billette, F. & Lambare, G., 1998. Velocity macro-model estimation from seismic reflection data by stereotomography, *Geophys. J. Int.,* **135,** 671–690.

Billette, F., Le Bégat, S., Podvin, P. & Lambare, G., 2003. Practical aspects and applications of 2D stereotomography, *Geophysics,* **68,** 1008–1021.

Bube, K.P. & Langan, R.T., 1994. A continuation approach to regularization for traveltime tomography, *SEG Tech. Prog. Exp. Abstr.,* **13,** 980–983.

Cao, D., Hirabayashi, N., Leaney, S., Borland, W., Hara, K. & Johnston, P., 2000. An integrated 3-D tomographic inversion – Application to multi-survey VSP data, *SEG Tech. Prog. Exp. Abstr.,* **19,** 1779–1782.

Chiu, S.K.L. & Stewart, R.R., 1987. Tomographic determination of three-dimensional seismic velocity structure using well logs, vertical seismic profiles, and surface seismic data, *Geophysics,* **52,** 1085–1098.

Chopra, S., Blias, E., Manerikar, A., Kryzan, A., Chavina, L., Alexeev, V. & Larsen, G., 2002. Simultaneous acquisition of 3D surface seismic and 3D VSP data—processing and integration, *SEG Tech. Prog. Exp. Abstr.,* **21,** 2337–2340.

Constance, P.E., Holland, M.B., Roche, S.L., Bicquart, P., Bryans, B., Gelinsky, S., Ralph, J.G. & Bloor, R.I., 1999. Simultaneous acquisition of 3-D surface seismic data and 3-C, 3-D VSP data, *SEG Tech. Prog. Exp. Abstr.,* **18,** 104–107.

Gosselet, A., Le Bégat, S. & Petersen, S.A., 2004. Slope transmission tomography for borehole positioning, *SEG Tech. Prog. Exp. Abstr.,* **23,** 2331–2334.

Lapin, S., Kisin, S. & Zhou, H.-W., 2003. Joint VSP and surface seismic tomography, *SEG Tech. Prog. Exp. Abstr.,* **22,** 2342–2344.

Leaney, S., Tcherkashnev, S., Wheeler, M., Idrees, M., Hastings, A., Touami, M., Mekmouche, S. & Kasmi, R., 2003. In-line walkaway processing and integration, *SEG Tech. Prog. Exp. Abstr.,* **22,** 2203–2206.

Le Bégat, S., Podvin, P. & Lambaré, G., 2000. Stereotomography : strategy for application to real data in 2D, in *Proceedings of 62nd annual meeting (Extended Abstracts),*Eur. Ass. Geosc. Eng, L46.

Le Bégat, S., Chauris, H., Devaux, V., Nguyen, S. & Noble, M., 2004. Velocity model estimation for depth imaging: comparison of three tomography methods on a 2D real data set, *Geophys. Prosp.,* **52**(5), 427–438.

Nguyen, S., Noble, M., Thierry, P. & Baina, R., 2002. Tomography picking in the depth migrated domain using migration of attributes, *SEG Tech. Prog. Exp. Abstr.,* **21,** 963–966.

Ory, J. & Pratt, R.G., 1995. Are our parameter estimators biased? The significance of finite-difference regularization operators, *Inv. Prob.,* **11,** 397–424.

Paige, C.C. & Saunders, M.A., 1982. LSQR: an algorithm for sparse linear equation and sparse least squares, *ACM Trans. Math. Software,* **8,** 43–71.

Pratt, G. & Chapman, C.H., 1992. Traveltime tomography in anisotropic media—II. Application, *Geophys. J. Int.,* **109,** 20–37.

Riabinkin, L.A. 1957. Fundamentals of resolving power of controlled directional reception (CDR) of seismic waves, in *Slant-stack Processing,* Geophysics Reprints 14, Gardner G.H.F. & Lu, L., eds, pp. 36–60, Soc. Expl. Geophys., Tulsa, Ok.

Robein, E., 2004. *Velocities, Time-imaging and Depth-imaging: Principles and Methods,* EAGE Publications BV, Houten, the Netherlands.

Rossi, G., Corubolo, P., Bohm, G., Ceraggioli, E., Dell'Aversana, P., Morandi, S., Poletto, F.P. & Vesnaver, A., 2001. Joint 3-D inversion of SWD and surface seismic data, *First Break,* **19,** 453–459.

Sen, M.K. & Roy, I.G., 2003. Computation of differential seismograms and iteration adaptive regularization in prestack waveform inversion, *Geophysics,* **68,** 2026–2039.

Sexton, P., 1998. 3D velocity-depth model building using surface seismic and well data, *PhD thesis*. University of Durham, England.

Sword, J.C.H., 1986. Tomographic determination of interval velocities from picked reflection seismic data, *SEG Tech. Prog. Exp. Abstr.,* **5,** 657–660.

Tarantola, A., 1987. *Inverse Problem Theory : Method for Data Fitting and Model Parameter Estimation,* Elsevier, Amsterdam.

Vesnaver, A., Bohm, G. & Galuppo, P., 1999a. Staggered versus adapted grids for the joint 3D inversion of surface and well data, *SEG Tech. Prog. Exp. Abstr.,* **18,** 1793–1796.

Vesnaver, A.L., Bohm, G., Madrussani, G., Petersen, S.A. & Rossi, G., 1999b. Tomographic imaging by reflected and refracted arrivals at the North Sea, *Geophysics,* **64,** 1852–1862.

Wang, B., 1993. Improvement of seismic travel-time inversion methods and application to observed data. *PhD thesis*. Purdue University, West Lafayette.

Whiting, P., 1998. Reflection tomography without picking, *SEG Tech. Prog. Exp. Abstr.,* **17,** 1226–1229.

Xu, S., Chauris, H., Lambare, G. & Noble, M., 2001. Common-angle migration: a strategy for imaging complex media, *Geophysics,* **66,** 1877–1894.